Imaging plant tissues: advances and promising clearing practices

Mathilde Hériché, Christine Arnould, Daniel Wipf, Pierre-Emmanuel Courty

Clearing plant tissues: advances and promising practices

Mathilde Hériché[1], Christine Arnould[1], Daniel Wipf[1], Pierre-Emmanuel Courty[1]

0000000268230836 @m_heriche

0000000327897818 @pecourty21/@Radiomyco

0000000171975612 @wipf1967

[1]Agroécologie, AgroSup Dijon, CNRS, Univ. Bourgogne, INRAE, Univ. Bourgogne Franche-Comté, Dijon, France

Correspondence: pierre-emmanuel.courty@inrae.fr (P.E. Courty)

Keywords: plant, clearing, light absorption and scattering, refractive index, optical sectioning microscopy, 3D imaging

Abstract

The study of the organ structure of plants and understanding their physiological complexity requires 3D imaging with subcellular resolution. Most plant organs are highly opaque to light, therefore their study under optical sectioning microscopes is difficult. In animals, many protocols have been developed to make organs transparent to light using clearing protocols (CPs). By contrast, clearing of plant tissues is a challenge due to the presence of fibres and pigments. In this review, we describe how progress of plant CPs was achieved throughout the past twenty years by an adapted taxonomy, implemented by physical and optical parameters affecting tissue properties. We also discuss successful approaches combining CPs and promising microscopy methods and their future applications in plant science research.

Aim to observe in depth plant tissues

Since Hooke's first observation and description of cork cuts in the middle of the 17th century, plant science research has remained closely related to advances in optical microscopy. More specifically, the use of fluorescence labeling and optical sectioning has drastically improved the understanding of tissue micromorphology [1], cell development [2], protein localization and plant-microbe interactions [3]. These microscopy approaches are, however, limited to approximately 30 µm depth because of the opacity and auto-fluorescence of plant tissues. Opacity is mainly due to (i) light absorption by pigments, and (ii) light scattering by the wide range of **Refractive Indices** (**RI**, see Glossary) of cell components (Figure 1). Moreover, plants contain a lot of light-sensitive pigments and aromatic compounds that animal tissues do not have. These compounds can react to laser excitation from microscope and generate a significant noise impairing the fluorescent signal of interest. Two approaches are available to overcome limitations related to depth and chemical composition. The usual approach consists in mechanical sectioning. This type of sample preparation is time consuming, section borders can be damaged (causing a loss of cell content) and 3D reconstruction can be approximate, leading to a loss of information [4]. Another approach consists in clearing sample by chemical treatments. Clearing protocols (CPs) make sample transparent to light by (i) removing light-active compounds, and (ii) homogenizing RI inside plant tissue (Box 1). This process allows the acquisition of a fluorescent signal through a thick sample. Over the past twenty years, many CPs have been

developed for animal tissues (*e.g.* zebrafish, mouse), mainly in neuroscience to study brain tissues; followed by application to other organs, including bones, up to the whole body [5].

Here, we review all CPs that have been applied and adapted from animal-based observation or specifically developed for plant tissues to gain new insights into plant physiology and develop prospects in the field. First, we apply the CPs classification in force based on organic solvents and aqueous solutions with passive immersion, protein hyperhydration and hydrogel embedding. Next, we discuss briefly chemical and physical impacts of CPs on tissue properties. Finally, we present successful CPs that have been applied to animals tissues and combined with recently developed microscopy techniques for being further transferred and optimized on plant organs. We aim to provide helpful guidance for scientists to select the most appropriate CP among existing ones, or to develop their own clearing approach, depending on plant tissue and scientific issue.

A glimpse of the historical record of clearing reagents

The work of Spalteholz in 1911 [6] was one of the first record to have used clearing agents on human organs. In plant research, lactic acid [7] and chloral hydrate [8,9] initially used as a mounting and preserving medium in Hoyer's solution [10], were two commonly used clearing agents. Their ability to clear tissues relies on their RI of 1.43, very close to plant cell wall RI (1.42). Chloral hydrate has been used in many CPs on a wide range of plants, especially on *Arabidopsis thaliana* (*A. thaliana*), to clear various organs (*e.g.* the phloem [11], leaves [12], flower organs and siliques [13]), and in combination with diverse fixation techniques and staining agents (*e.g.* acid fuchsin [8], aniline blue [14], GUS [11]). In fluorescence-based microscopy, chloral hydrate has been combined with the fluorescence of modified **Pseudo-Schiff reagents** - Propidium Iodide (m**PS**-PI) to visualize the plant cell wall [12]. Nevertheless, chloral hydrate treatment leads to endogenous fluorescence quenching, that made it not very popular [15] in addition to its anaesthetic effect.

The need to observe plant tissues in depth has led to the independent development of many CPs depending on the sample (*e.g.* reproductive organs [16]), structure of interest (*e.g.* lignin [17]) and timescale (*e.g.* one-step clearing [18]). Gardner summarized CP steps such as fixation, alkali dissolution, post-alkali treatment, depigmentation, crystal removal, high-RI solution and staining [19]. Until then, microscopes used for such observations had not reached subcellular-level resolution. Advances in optical sectioning microscopy (confocal,

two-photon, light sheet microscopes) and increasing contrast and resolution paved the way for many CPs that allowed **Fluorescent Probes** (**FP**) imaging.

Clearing protocols for plant tissues

Recent animal CPs are usually classified into two main categories based on physicochemical properties of clearing agents: (i) organic solvents and (ii) aqueous solutions [20]. What about plant CPs for FP imaging?

Solvent-based clearing

The pioneer CP [6] followed a procedure that was standardized and described in animals: dehydration, lipid solvation and incubation in a high RI solution [21]. Few recent methods have been described in animal research, especially for brain tissue [22], but the literature about plant research is poorly documented.

Littlejohn et al. used perfluorocarbons as a mounting medium to observe *A. thaliana* leaves by confocal microscopy. Although the authors never employed the term “clearing” in the development of this protocol over the years [23,24], their approach relied on the homogenization of the sample RI (Box 1). The RI of perfluoroperhydrophenanthrene (PP11, 1.334) is very close to the RI of cytoplasm (1.35 – 1.39), but far from the RI of air (1.00). Littlejohn et al. had to deal with the spongious mesophyll of *A. thaliana* leaves, meaning that they needed an agent able to replace air in leaf cavities and with a RI close to that of cytoplasm in order to ensure the path of light through leaf tissue. Using this reagent, they successfully cleared non-fixed leaves in 10 min and succeeded in observing a GFP signal at a depth of 75 µm[24]. This low RI solution, however, has never been applied to any other plant organ [25].

The story of Visikol™ started in 2013, when Villani and colleagues [26] published the efficiency of this new clearing agent formulation (RI = 1.445) designed to replace chloral hydrate, and successfully tested on small plant samples (fresh or dried). The clearing step consisted in heating (60-80°C) sample in Visikol™ on a slide for less than one minute. Visikol™ was compared with chloral hydrate and potassium hydroxide, using different mounting media, under confocal and airyscan microscopes [27]. They treated leaves for 3 to 24 hrs with Visikol™ at 40°C to observe cuticle stained by PI. Visikol™ won the game thanks

to its nontoxicity and affordability. Later on, *A. thaliana* root tips were cleared using Visikol™ and successfully stained by GUS histochemical labeling (CyclinB1;1-GUS, [28]).

The benzyl benzoate/benzyl alcohol mixture (1:2 (v:v) **BABB**; RI = 1.559) – a widely used clearing agent in animal CPs – has been little used in plant CPs. BABB was used to initially image *A. thaliana* under Optical Projection Tomography (OPT) [29] before the authors improve their instrument to perform a macro-OPT (M-OPT, see section 2) to image *A. thaliana* veins by GUS staining in 3D in an entire plant [30]. Plants were fixed in acetone for 20 min, GUS-stained, dehydrated (methanol, 1 week), cleared and mounted in BABB. Galls caused by nematodes were studied on *A. thaliana* roots [31]. They performed glutaraldehyde fixation (overnight), ethanol dehydration (overnight), clearing and mounting in BABB to visualize a complete gall structure with a nematode in 3D only by recording the autofluorescence signal on a laser scanning confocal microscope. In fact, both protocols induced severe fluorescence quenching and BABB potentially induced rapid peroxide contamination that damaged FP [32]. In the latest version of the protocol – FluoClearBABB –, the dehydration step is modified (*tert*-butanol, 7 days) and a basic pH (9.5) is maintained [33]. This CP allowed the authors to record enhanced Green Fluorescent Protein (eGFP) signals in an entire mice brain under a home-built light sheet fluorescent microscope. Unfortunately, this CP is not referenced yet in plant tissue literature.

Methyl salicylate, another widely used clearing agent (RI 1.53) [6,34], has recently been combined with FP imaging. On *Zea mays* ovules, Kalinowska and colleagues performed a formalin-acetic acid-alcohol fixation (FAA, various concentrations and time depending on organs) and made Feulgen staining (hours). Then, they made a gradual ethanol dehydration (hours) before clearing in methyl salicylate (hours) [35]. They observed on a confocal microscope a good level of transparency on these very dense organs at different stage of development, but no acquisition in *z* was reported. González-Gutiérrez and colleagues, fixed Crassinucellate ovules (formaldehyde (FA)), permeabilized membranes and cuticles (acetone), stained tissues by rhodamine-phalloidin (F-actin marker) and Hoescht (nuclei marker), dehydrated (isopropanol) and cleared (methyl salicylate) tissues. In their study, authors precise that this CP can be done in 48 hrs [36]. Under a confocal microscope, they successfully imaged actin network of entire ovule but once again, no acquisition in *z* was reported. This year, He and colleague [37] developed a new CP for crop roots based on

methyl salicylate. They proceed to a fixation step (15.5 hrs) with paraformaldehyde (PFA) and dimethylsulfoxide (DMSO), an RNAse treatment (12hrs), a PI staining (overnight), a dehydration step in ethanol (4 hrs) and at least clearing by methyl salicylate immersion (overnight). Under a confocal microscope, they successfully imaged PI fluorescent signal on entire rice root tips thickness, but endogenous GFP signal were lost.

Due to dehydration step, solvent based CPs are known to induce shrinkage on soft tissues [5]. In the literature cited above, this phenomenon is not reported except for thin root tips of *A. thaliana* [37]. It can be explained by the presence of cell walls in plant tissue, but more studies are needed to confirm the absence of shrinkage during clearing of whole organs.

Aqueous-based clearing

Hydrophilic CPs involve three techniques: passive immersion, protein hyperhydration and hydrogel embedding. A wide range of aqueous-based protocols developed on animal tissue have been adapted to plants. Aqueous-based CPs are compatible with FPs but are relatively time-consuming compared to solvent-based CPs [5].

In simple immersion, the lipid content of the sample is preserved. This CP consists in matching the RI of lipid tissue (that is greater than 1.45 in animals) thanks to aqueous solutions with a high RI solution [21].

The See Deep Brain (SeeDB) is a mixture of fructose (80.2% w/w) and 0.5% α-thioglycerol, and a known efficient clearing agent on brain tissue [38]. It was tested on various plant leaves, including tree leaves [39]. One-cm diameter leaf discs were drop fixed in FAA, cleared in SeeDB by immersion (1-3 days), and stained with PI and calcofluor white. SeeDB was not as efficient as other tested chemical reagents such as 1% sodium hypochlorite (NaClO) on leaves. This publication is liable to criticism because (i) the chemical reaction of NaClO into the tissue is not detailed and (ii) even if NaClO is not recording as a clearing agent in animals, it has already been applied on plant leaves [40].

2,2'-thiodiethanol (TDE) was first used as a mounting medium [41]. Its high RI is proportional to its concentration (1.374 - 20%; 1.515 - 97%) and makes it an effective, user-friendly clearing agent, suitable for various microscopy systems and samples [42,43]. In plant tissues, TDE was used in a CP called Transparent plant Organ MEthod for Imaging (TOMEI) to

clear *A. thaliana* and *Oryza sativa* organs [44]. Without sectioning and with a fixation step based on acetic acid:ethanol (1:3, 1-2hrs, TOMEI-I) or PFA (4%, 1hr, TOMEI-II), they analyzed cell structures at a depth of 200 µm in a few hours. In *A. thaliana*, fixation with 4% PFA turned out to be a necessary step before using TDE to avoid tissue disruption and FP quenching [45]. Whatever the fixation step, a high concentration of TDE (95% - 100%) can weaken the fluorescent signal of some endogenous FP (*e.g.* Venus-YFP and eGFP are more sensitive to quenching than mCherry and Citrine-YFP), and lead to a loss of tissue integrity. These authors also determined that a 50% - 70% TDE solution was necessary and sufficient to clear challenging plant tissues while preserving the structure and the fluorescent signal. Nevertheless, later comparative studies revealed that TOMEI doesn't remove all pigments and can decrease FP intensity [45]. To overcome these limitations, an update of this CP, called iTOMEI (improved TOMEI) was published in 2021 [46]. They convey a large screening of chemical treatments for each CP steps based on (i) preservation of GFP signal, (ii) enhancement of GFP signal and (iii) clearing efficiency. After comparison, they proposed a fixation step with 1% FA in PBS buffer, a decolourization step with 20% caprylyl sulfobetaine (a detergent) in sodium phosphate buffer at pH 8.0 and a clearing step with 70.4% iohexol instead of TDE. They successfully imaged entire *A. thaliana* seedlings, organs of *O. sativa* and *Marchantia polymorpha* at a depth of 80µm and 200µm respectively, under confocal or two photons microscopes. RI of the solutions was not provided, but iohexol solution seems to be prepared in the same buffer and at the same concentration as in SeeDB2 CP (an upgrade of SeeDB CP) [47]. In iTOMEI, detergent is used to improve chlorophyll elution, so iTOMEI is not just a "simple immersion" CP as TOMEI is. Nonetheless, as SeeDB2 required saponin as a detergent and is still classified into "simple immersion" category in animal CP taxonomy [5], we chose to keep iTOMEI in this category (Figure 2). Concerning caprylyl sulfobetaine, it is referenced as a zwitterionic detergent solvating oleosins. Hence, we can easily ask for the impact of iTOMEI on protein and lipid contents of cleared sample.

Another approach consists in decreasing and then homogenizing the RI of a sample in two steps: (i) removal of lipid content (delipidation) and (ii) hyperhydration of proteins. In order to maintain an aqueous-based environment to support FP activity, delipidation is performed using a detergent. This step is longer compared to delipidation with an organic solvent (weeks to months *versus* hours) [21]. Following delipidation using Triton X and

hyperhydration using urea, the Sca*l*e technique decreased the RI of mouse brain tissue to 1.38 [48]. In plants, delipidation using Triton X in glycerol was combined with urea on leaves (*Zea mays*, *Medicago truncatula*, *Nicotiana benthamiana*, *Pisum sativum*) and nodules of leguminous plants (*P. sativum*) [49]. Fixation was achieved using PFA or glutaraldehyde. The staining step was adapted according to plant tissue (Table 1). Warner and colleagues [49] succeeded in imaging a fluorescent signal at more than 350µm depth on intact nodules and immunolabeling sections of cleared nodules (by adding an enzymatic digestion step to the CP). Recently, this CP has been used to clear *Lotus japonicus* roots and nodules to visualize auxin and cytokin dynamics and cell division patterns with cellular resolution during nodulation thanks to markers optimized for fluorescent and bright field microscopy [50]. Following Warner's pattern of combining polyhydric alcohol, detergent and urea. Kurihara et al. [15] carried out a large chemical screening. It was based on (i) the clearing efficiency of different compounds from the literature (especially efficient to remove chlorophyll autofluorescence), (ii) the suitability of this compound with recombinant Venus fluorescence, and (iii) the clearing efficiency of mixtures containing selected compounds and detergents. They concluded that ClearSee (xylitol/sodium deoxycholate/urea) has a good clearing efficacy, and was suited for a large range of endogenous FPs (*e.g.* mTFP1, sGFP, mClover, Venus, mCitrine, tdTomato, mApple), numerous organs (leaves, roots, seedlings, pistils, stems and protonemata) and plant species (*A. thaliana, Physcomitrella patens*). Since then, ClearSee has been applied to a wide range of plant species and organs [51–55]. Nagaki and colleagues [56] optimized the initial ClearSee method for immunohistochemistry (namely ePro-ClearSee). They added an enzymatic digestion step by cellulase and pectolyase, and a 2-propanol treatment step (permeabilization) before clearing (timescale: 10 days to 3 weeks). Using confocal microscope with or without airyscan detector, they acquired a fluorescent signal from modified immunolabeled histones in leaves and roots of various plant species. In the latest update of this protocol, named ClearSeeAlpha, a reductant (sodium sulfite 50 mM) was added to avoid brown pigmentation due to polyphenol oxidation [57]. These authors successfully cleared brown-pigmentation-sensitive leaves and floral organs of various plant species. Moreover, using a multiphoton confocal microscope, they demonstrated the suitability of this protocol with endogenous FPs. By combining a depigmentation step previously developed on Xenopus [58], an enzymatic digestion based on ePro-ClearSee and a clearing step with ClearSeeAlpha, the Clearing

Tannic Roots (CTR) protocol enabled acquisition of a PI signal on entire *Vitis vinifera* root thickness (250µm in z) under a confocal microscope [59]. Authors noticed that the time required has to be adapted according to root age : the older the tissue, the longer each step takes.

To avoid potential removal of key structural proteins by solvents and concentrated detergents, Chung and colleagues [60] introduced another aqueous CP, consisting in fixing and embedding the sample in a polyacrylamide hydrogel. Combined with a low-concentrated Sodium Dodecyl Sulfate solution (SDS 8%) and electrophoresis, the **CLARITY** method removed lipids and other light-active compounds. In plant tissues, Palmer and colleagues [61] added an enzymatic degradation step to the passive CLARITY protocol to clear *Nicotiana tabacum* leaves. They called their method Plant-Enzyme-Assisted CLARITY (PEA-CLARITY). The enzyme cocktail (cellulase, xylanase, arabinofuranosidase, pectate lyase and α-amylase) is directed against cell wall to enhance its permeability to fluorescent dyes, especially antibodies, for better immunolabeling efficiency. The hydrogel embedding medium prevents tissue collapse by providing a supportive network. Finally, RI homogenization is done by immersion in a high RI solution like TDE [62], and can record the fluorescent immunolabeled signal of an entire tobacco leaf (200 µm depth)(Table 1).

Aqueous based CPs are well described to induce swelling of soft samples. While expansion phenomenon is used in animal cleared organ to gain in resolution [63], its use in plant organs is still not reported, probably because of plant cell wall. A large part of aqueous based-CPs, however, was developed to modify and elute cell components (*e.g.* complex sugars, proteins and lipids). According to the treatment strength, a tissue can loss its integrity and become weaker [62].

Optical clearing methods serving optical sectioning techniques

Until the middle of the twentieth century, in-depth observation of tissues was still limited by the efficiency of fluorescence microscopes. When observing a thick sample on a standard fluorescence microscope, only the surface could be imaged. In depth, the signal in focus was blurred by the out-of-focus fluorescent signal of the rest of the sample. The challenge of optical sectioning was to remove this out-of-focus background. The

development of computer-aided optical sectioning microscopy paved the way for 3D microscopy and promoted clearing agent applications [32].

Optical sectioning consists in selecting a specific (*x*, *y*) plane and in acquiring this plane at multiple depths. The acquired images are called *z*-stacks; the lower the interval between *z*-stacks, the higher *z* resolution. Optical sectioning developed along with the use of confocal microscopy. This technique is based on wide-field illumination; thanks to the pinhole, only photons emitted from the focal plan are collected, leading to removal of the out-of-focus background. Photon dispersion, however, increases with depth of acquisition [64]. This is one of the reasons why confocal microscopy of thick samples is highly dependent on CP. Another way of avoiding the out-of-focus background is to avoid generating it through specific illumination. Two-photon and light sheet illumination were designed to answer this question. Compared to confocal microscopy, imaging process is faster and less phototoxic [65] [66]. **Light Sheet Fluorescence Microscopy** (**LSFM**) has many applications combined with clearing agents, hence different names across publications (Box 2). Silvestri and colleagues [20] present a complete overview of CPs adapted for each of the three types of microscopy techniques (confocal, two-photon and LSFM) according to their physical principles.

Moreover, another factor impacting depth imaging are spherical aberrations [67]. These aberrations are evaluated by the **Point Spread Function** (**PSF**) that described the image of a single point through an optical system, called convolution. This function determined the resolution of an optical system (each microscopy type has its own shape type of PSF) and PSF depends on the RI of the entire imaging system. Even if CP aim to homogenise RI between tissue and embedding medium, mismatch between RI of the objective medium lens and clearing solution generate aberrations, leading to an extended PSF and a decrease in spatial resolution [67]. To deal with this problem, microscope manufacturer could propose either objectives with correction RI collar or specific objective matching clearing solution RI [68]. Moreover, two numerical criteria can be calculated to predict the loss of image quality and the best objective to use according to the clearing agent [69]. A post computational treatment, called deconvolution, can also be applied to lower aberrations. This operation reassigns the aberrated light to its original source thanks to the theorical PSF of the optical system (*e.g.* Huygens software).

Even if LSFM is the most widely used microscope technique, cleared tissue can be imaged with a wide range of microscopes.

Optical projection tomography (OPT) is an adaption of tomography from X-ray imaging to optical systems [70]. In this system, the entire sample is placed in a cylinder and rotated during acquisition. Light transmission images – called projections or tomographic sections – are collected in different directions. Then, 3D reconstruction based on that projection is done using an algorithm [71]. The technique is compatible with fluorescence, and the system is known as emission OPT [72]. OPT systems are highly sensitive to tissue scattering, so that their optimization is closely related to the development of clearing agents. Lee and colleagues [29] first observed BABB-cleared *A. thaliana* various organs under an OPT system but they could not go beyond 15 mm depth. Consequently, they published an article about a Macro-OPT (M-OPT) system in 2016 [30] that allowed 3D imaging of very large specimens (up to 60 mm tall and 45 mm deep) and could be used with any clearing agent (resolution range : from 6.5 to 62.5 µm/voxel). Here, M-OPT is not reported to image FP signal in cleared plant tissue. Nevertheless, as OPT is suitable with fluorescent imaging and, new user-friendly hardware and software are available [73], M-OPT promises new insight deep volume imaging in cleared plant tissue.

Other devices have been used with clearing agents, but still not applied to plant tissue.

Stimulated Raman Scattering microscopy (micro-**SRS**) is a recent microscopy technique based on the combination of optical microscopy and Raman spectroscopy. This instrument can map chemical bonds in 3D, with subcellular resolution, but laser emission is sensitive to scattering, and depth imaging is limited to 100 µm [74]. To solve this problem, CPs suitable with Raman spectroscopy were designed to achieve lipid and protein mapping of brain tissue across 1 mm depth [74] and to image collagen and hydroxyapatite during skull clearing process [75]. Micro-SRS was first used on *A. thaliana* leaves [76], and then to study the chemical composition of cuticular waxes and cell walls, and to investigate agrochemicals in maize and cotton leaves [77]. The authors, however, did not mention any acquisition deep into the tissue, and micro-SRS applied to cleared plant samples is still lacking.

Hyperspectral dark field microscopy images nanoparticles based on their refractive spectral signature. In this way, it is possible to label many biological structures of interest (*e.g.*, mRNA, membrane proteins) with plasmonic nanoparticles (metals). Although contrast

in dark field microscopy is generated by tissue scattering, the plasmonic signal is impaired by this background [78]. By clearing human cells (*in vitro* lines), the signal-to-noise ratio of gold nanoparticles is 5 to 6 times greater, so that monomeric and oligomeric forms of transmembrane receptors can be distinguished and mRNA can be detected at single copy-resolution [78]. At tissue scale, clearing human skin samples allowed 2D and 3D mapping of plasmonic nanoparticles signals, and improved the signal to noise ratio [79]. Many studies exist on tracing metal particles in animal tissues *via* this microscopy technique, but clearing process are not routinely applied [80]. Concerning plant tissues, *A. thaliana* roots and various legume leaves have been analyzed under a hyperspectral dark field microscope to image gold and iron particles, respectively, after exposure during germination [81,82]. Once again, no CP has been reported for these tissues.

STimulated Emission Depletion (STED) is a super-resolution microscopy technique based on the destruction of the fluorescence emission signal around the initial point of laser excitation. Many parameters can be modulated on a STED microscope, including implantation with other optical techniques, to overcome the specific constraints imposed by sample specificities and image them in 3D [83]. Like all optical fluorescence microscopes, however, it is highly sensitive to light scattering and spherical aberrations and can be easily combined with a CP when using fixed tissue. By adapting the SeeDB-based protocol to super resolution microscopy (SeeDB2), FPs signal was acquired through a commercial STED microscope (chemical fluorophores and fluorescent proteins) in mouse brain down to 100 µm depth, with 50 nm lateral resolution [47]. Angibaud and colleagues [84] cleared mouse brain using **CMF3** (RI = 1.518) and imaged it by a STED immunofluorescent signal at a depth of 40 µm. As Komis and colleagues mentioned [85] in their review, observation of plant tissues by STED techniques are very challenging . One of their outstanding questions – how to overcome the light-scattering properties of bulk plant samples with greatly varying refractive indices in the axial direction – could probably be answered by an adapted CP [86].

Concluding remarks

CPs have already provided new insights into plant tissues and chlorophyllous organs. But, no single plant CP can suit all imaging projects because of plant tissues and organs diversity. Further optimization on organs containing certain light active compounds (*e.g.* phenols) is

needed [87]. Therefore, future CPs will have to be based on systematic chemical screening because all organs vary in their lipid, protein and sugar compositions. Moreover, comparative studies of various CPs applied on the same organ are necessary to evaluate the most suited one with an emphasis on CPs compatible with specific fluorescent dyes (*e.g.* immunofluorescence [88]). Compared to publications on animal tissues [89], the field of CPs on plant tissue is still in its early stages, but it is promising approach to unravel anatomical and physiological insights in plant-microbes interactions (see Outstanding Questions). CPs need to be seen in the context of studying plant physiology at different scales, from the entire plant down to the organ level and from the cell to the protein network.

Acknowledgements

The authors thank the Burgundy Franche Comté Regional Council. Mathilde Hériché receives a doctoral contract accredited by the French Ministry of Higher Education, Research and Innovation. The authors also thank Antoine Sportes for discussions.

References

1 Wei, J. *et al.* (2020) Low-cost and efficient confocal imaging method for arabidopsis flower. *Developmental Biology* 466, 73–76

2 Prunet, N. (2017) Live Confocal Imaging of Developing Arabidopsis Flowers. *JoVE* DOI: 10.3791/55156

3 Harrison, M.J. *et al.* (2002) A Phosphate Transporter from Medicago truncatula Involved in the Acquisition of Phosphate Released by Arbuscular Mycorrhizal Fungi. *The Plant Cell* 14, 2413–2429

4 Atkinson, J.A. and Wells, D.M. (2017) An Updated Protocol for High Throughput Plant Tissue Sectioning. *Front. Plant Sci.* 8, 1721

5 Matryba, P. *et al.* (2019) Advances in Ex Situ Tissue Optical Clearing. *Laser & Photonics Reviews* 13, 1800292

6 Spalteholz, W. (1911) Uber das Durchsichtigmachen von menschlichen und tierischen Pr¨aparaten und seine theoretischen Bedingungen. *S. Hirzel, Leipzig*

7 Simpson, J.L.S. (1929) A Short Method of Clearing Plant Tissues for Anatomical Studies. null 4, 131–132

8 McBryde, M.C. (1936) A METHOD OF DEMONSTRATING RUST HYPHAE AND HAUSTORIA IN UNSECTIONED LEAF TISSUE. *American Journal of Botany* 23, 686–688

9 Lersten, N. R. (1967) An annotated bibliography of botanical clearing methods. *Iowa State Journal of Science* 41, 481 – 486

10 Anderson, L.E. (1954) Hoyer's Solution as a Rapid Permanent Mounting Medium for Bryophytes. *The Bryologist* 57, 242

11 Truernit, E. *et al.* (2008) High-Resolution Whole-Mount Imaging of Three-Dimensional Tissue Organization and Gene Expression Enables the Study of Phloem Development and Structure in Arabidopsis. *Plant Cell* 20, 1494–1503

12 Wuyts, N. *et al.* (2010) High-contrast three-dimensional imaging of the Arabidopsis leaf enables the analysis of cell dimensions in the epidermis and mesophyll. *Plant methods* 6, 17
13 Hedhly, A. *et al.* (2018) Whole-mount Clearing and Staining of Arabidopsis Flower Organs and Siliques. *JoVE* DOI: 10.3791/56441
14 Bougourd, S. *et al.* (2000) An aniline blue staining procedure for confocal microscopy and 3D imaging of normal and perturbed cellular phenotypes in mature Arabidopsis embryos. *The Plant Journal*
15 Kurihara, D. *et al.* (2015) ClearSee: a rapid optical clearing reagent for whole-plant fluorescence imaging. *Development* 142, 4168–4179
16 Stebbins, G.L. (1938) A Bleaching and Clearing Method for Plant Tissues. *Science* 87, 21–22
17 Li, Y. *et al.* (2016) Optically Transparent Wood from a Nanoporous Cellulosic Template: Combining Functional and Structural Performance. *Biomacromolecules* 17, 1358–1364
18 Herr, J.M. (1971) A New Clearing-Squash Technique for the Study of Ovule Development in Angiosperms. *American Journal of Botany* 58, 785–790
19 Gardner, R.O. (1975) An overview of botanical clearing technique. *Stain Technol* 50, 99–105
20 Silvestri, L. *et al.* (2016) Clearing of fixed tissue: a review from a microscopist's perspective. *JBO* 21, 081205
21 Richardson, D.S. and Lichtman, J.W. (2015) Clarifying Tissue Clearing. *Cell* 162, 246–257
22 Neuhaus, B. *et al.* (2017) Collection management and study of microscope slides: Storage, profiling, deterioration, restoration procedures, and general recommendations. *Zootaxa* 4322, 1
23 Littlejohn, G.R. and Love, J. (2012) A Simple Method for Imaging Arabidopsis Leaves Using Perfluorodecalin as an Infiltrative Imaging Medium. *JoVE* DOI: 10.3791/3394
24 Littlejohn, G.R. *et al.* (2014) An update: improvements in imaging perfluorocarbon-mounted plant leaves with implications for studies of plant pathology, physiology, development and cell biology. *Front. Plant Sci.* 5,
25 Timmers, A.C.J. (2016) Light microscopy of whole plant organs: LIGHT MICROSCOPY OF WHOLE PLANT ORGANS. *Journal of Microscopy* 263, 165–170
26 Villani, T.S. *et al.* (2013) An Improved Clearing and Mounting Solution to Replace Chloral Hydrate in Microscopic Applications. *Applications in Plant Sciences* 1, 1300016
27 Urban, M.A. *et al.* (2018) Cuticle and subsurface ornamentation of intact plant leaf epidermis under confocal and superresolution microscopy. *Microsc. Res. Tech.* 81, 129–140
28 Ashraf, M.A. and Rahman, A. (2019) Cold stress response in *Arabidopsis thaliana* is mediated by GNOM ARF-GEF. *Plant J* 97, 500–516
29 Lee, K. *et al.* (2006) Visualizing Plant Development and Gene Expression in Three Dimensions Using Optical Projection Tomography. *The Plant Cell* 18, 2145–2156
30 Lee, K.J.I. *et al.* (2016) Macro optical projection tomography for large scale 3D imaging of plant structures and gene activity. *EXBOTJ* DOI: 10.1093/jxb/erw452
31 Cabrera, J. *et al.* (2018) A Phenotyping Method of Giant Cells from Root-Knot Nematode Feeding Sites by Confocal Microscopy Highlights a Role for CHITINASE-LIKE 1 in Arabidopsis. *IJMS* 19, 429
32 Pavone, F.S. and Shoham, S., eds. (2020) Handbook of neurophotonics, First edition.CRC Press, Taylor & Francis Group. Becker, K. *et al* Chapter 9
33 Schwarz, M.K. *et al.* (2015) Fluorescent-Protein Stabilization and High-Resolution Imaging of Cleared, Intact Mouse Brains. *PLoS ONE* 10, e0124650
34 AU - Gilleron, J. *et al.* (2020) Exploring Adipose Tissue Structure by Methylsalicylate Clearing and 3D Imaging. *JoVE* DOI: 10.3791/61640
35 Kalinowska, K. *et al.* (2020) Imaging of Embryo Sac and Early Seed Development in Maize after Feulgen Staining. In *Plant Embryogenesis: Methods and Protocols* (Bayer, M., ed), pp. 191–203, Springer US

36 González-Gutiérrez, A.G. *et al.* (2020) Simple Whole-Mount Staining Protocol of F-Actin for Studies of the Female Gametophyte in Agavoideae and Other Crassinucellate Ovules. *Front. Plant Sci.* 11, 384

37 He, Y. *et al.* (2021) *An Optical Clearing Technique to Visualize Internal Root Structure*, In Review.

38 Ke, M.-T. *et al.* (2013) SeeDB: a simple and morphology-preserving optical clearing agent for neuronal circuit reconstruction. *Nat Neurosci* 16, 1154–1161

39 Lu, L. *et al.* (2020) A rapid and effective optical-clearing technique for deep tissue fluorescence imaging in trees. *Trees* DOI: 10.1007/s00468-020-01957-0

40 Benatti, M.N. A simple clearing technique to aid in the recognition of cilia and rhizinae structure in the Parmeliaceae.

41 Staudt, T. *et al.* (2007) 2,2'-Thiodiethanol: A new water soluble mounting medium for high resolution optical microscopy. *Microsc. Res. Tech.* 70, 1–9

42 Aoyagi, Y. *et al.* (2015) A Rapid Optical Clearing Protocol Using 2,2'-Thiodiethanol for Microscopic Observation of Fixed Mouse Brain. *PLoS ONE* 10, e0116280

43 Costantini, I. *et al.* (2015) A versatile clearing agent for multi-modal brain imaging. *Sci Rep* 5, 9808

44 Hasegawa, J. *et al.* (2016) Three-Dimensional Imaging of Plant Organs Using a Simple and Rapid Transparency Technique. *Plant Cell Physiol* 57, 462–472

45 Musielak, T.J. *et al.* (2016) A Versatile Optical Clearing Protocol for Deep Tissue Imaging of Fluorescent Proteins in Arabidopsis thaliana. *PLOS ONE* 11, e0161107

46 Sakamoto, Y. *et al.* (2021) *Improved clearing method contributes to deep imaging of plant organs*, In Review.

47 Ke, M.-T. *et al.* (2016) Super-Resolution Mapping of Neuronal Circuitry With an Index-Optimized Clearing Agent. *Cell Reports* 14, 2718–2732

48 Hama, H. *et al.* (2011) Sca*l*e: a chemical approach for fluorescence imaging and reconstruction of transparent mouse brain. *Nature Neuroscience* 14, 1481–1488

49 Warner, C.A. *et al.* (2014) An Optical Clearing Technique for Plant Tissues Allowing Deep Imaging and Compatible with Fluorescence Microscopy1[W][OPEN]. *Plant Physiol* 166, 1684–1687

50 Nadzieja, M. *et al.* (2019) A Toolkit for High Resolution Imaging of Cell Division and Phytohormone Signaling in Legume Roots and Root Nodules. *Front. Plant Sci.* 10, 1000

51 Duman, Z. *et al.* (2020) Short De-Etiolation Increases the Rooting of VC801 Avocado Rootstock. *Plants* 9, 1481

52 Ho, W.W.H. *et al.* (2020) Integrative Multi-omics Analyses of Barley Rootzones under Salinity Stress Reveal Two Distinctive Salt Tolerance Mechanisms. *Plant Communications* 1, 100031

53 Chen, M. *et al.* (2021) VAPYRIN attenuates defence by repressing PR gene induction and localized lignin accumulation during arbuscular mycorrhizal symbiosis of *Petunia hybrida*. *New Phytol* 229, 3481–3496

54 Eliyahu, A. *et al.* (2020) Vegetative propagation of elite Eucalyptus clones as food source for honeybees (Apis mellifera); adventitious roots versus callus formation. *Israel J. Plant Sci.* 67, 83–97

55 Kinoshita, A. *et al.* (2020) Expression Profiles of ANGUSTIFOLIA3 and SHOOT MERISTEMLESS, Key Genes for Meristematic Activity in a One-Leaf Plant Monophyllaea glabra, Revealed by Whole-Mount In Situ Hybridization. *Front. Plant Sci.* 11, 1160

56 Nagaki, K. *et al.* (2017) ePro-ClearSee: a simple immunohistochemical method that does not require sectioning of plant samples. *Scientific Reports* 7, 42203

57 Kurihara, D. *et al.* (2021) ClearSeeAlpha: Advanced Optical Clearing for Whole-Plant Imaging. *Plant and Cell Physiology* DOI: 10.1093/pcp/pcab033

58 Affaticati, P. *et al.* (2018) X-FaCT: Xenopus-Fast Clearing Technique. In *Xenopus* 1865 (Vleminckx, K., ed), pp. 233–241, Springer New York

59 Hériché, M. *et al.* (2021) New clearing protocol for tannic roots optical imaging. *Trends in Plant Science* DOI: 10.1016/j.tplants.2021.08.015

60 Chung, K. *et al.* (2013) Structural and molecular interrogation of intact biological systems. *Nature* 497, 332–337

61 Palmer, W.M. *et al.* (2015) PEA-CLARITY: 3D molecular imaging of whole plant organs. *Scientific Reports* 5, 13492

62 Palmer, W.M. *et al.* (2018) 3D Clearing and Molecular Labeling in Plant Tissues. In *Photosynthesis* 1770 (Covshoff, S., ed), pp. 285–304, Springer New York

63 Murakami, T.C. *et al.* (2018) A three-dimensional single-cell-resolution whole-brain atlas using CUBIC-X expansion microscopy and tissue clearing. *Nat Neurosci* 21, 625–637

64 Conchello, J.-A. and Lichtman, J.W. (2005) Optical sectioning microscopy. *Nat Methods* 2, 920–931

65 Helmchen, F. and Denk, W. (2005) Deep tissue two-photon microscopy. *Nat Methods* 2, 932–940

66 Mertz, J. (2011) Optical sectioning microscopy with planar or structured illumination. *Nat Methods* 8, 811–819

67 Silvestri, L. *et al.* (2014) Correcting spherical aberrations in confocal light sheet microscopy: A theoretical study: Aberrations in Light Sheet Microscopy. *Microsc. Res. Tech.* 77, 483–491

68 Marx, V. (2014) Microscopy: seeing through tissue. *Nat Methods* 11, 1209–1214

69 Asteriti, S. *et al.* (2020) Two simple criteria to estimate an objective's performance when imaging in non design tissue clearing solutions. *Journal of Neuroscience Methods* 332, 108564

70 Sharpe, J. (2002) Optical Projection Tomography as a Tool for 3D Microscopy and Gene Expression Studies. *Science* 296, 541–545

71 Haisch, C. (2012) Optical Tomography. *Annual Rev. Anal. Chem.* 5, 57–77

72 Walls, J.R. *et al.* (2007) Resolution improvement in emission optical projection tomography. *Phys. Med. Biol.* 52, 2775–2790

73 Vallejo Ramirez, P.P. *et al.* (2019) OptiJ: Open-source optical projection tomography of large organ samples. *Sci Rep* 9, 15693

74 Wei, M. *et al.* (2019) Volumetric chemical imaging by clearing-enhanced stimulated Raman scattering microscopy. *Proc Natl Acad Sci USA* 116, 6608–6617

75 Chen, Y. *et al.* (2019) Coherent Raman Scattering Unravelling Mechanisms Underlying Skull Optical Clearing for Through-Skull Brain Imaging. *Anal. Chem.* 91, 9371–9375

76 Littlejohn, G.R. *et al.* (2015) In Vivo Chemical and Structural Analysis of Plant Cuticular Waxes Using Stimulated Raman Scattering Microscopy. *Plant Physiol.* 168, 18–28

77 Mansfield, J.C. *et al.* (2013) Label-free Chemically Specific Imaging in Planta with Stimulated Raman Scattering Microscopy. *Anal. Chem.* 85, 5055–5063

78 Cui, Y. *et al.* (2016) Optical Clearing Delivers Ultrasensitive Hyperspectral Dark-Field Imaging for Single-Cell Evaluation. *ACS Nano* 10, 3132–3143

79 Touloumes, G.J. *et al.* (2020) Mapping 2D- and 3D-distributions of metal/metal oxide nanoparticles within cleared human ex vivo skin tissues. *NanoImpact* 17, 100208

80 Mehta, N. *et al.* (2021) DARK-FIELD hyperspectral imaging for label free detection of NANO-BIO-MATERIALS. *WIREs Nanomed Nanobiotechnol* 13,

81 Avellan, A. *et al.* (2017) Nanoparticle Uptake in Plants: Gold Nanomaterial Localized in Roots of *Arabidopsis thaliana* by X-ray Computed Nanotomography and Hyperspectral Imaging. *Environ. Sci. Technol.* 51, 8682–8691

82 Boutchuen, A. *et al.* (2019) Increased Plant Growth with Hematite Nanoparticle Fertilizer Drop and Determining Nanoparticle Uptake in Plants Using Multimodal Approach. *Journal of Nanomaterials* 2019, 1–11

83 Vicidomini, G. *et al.* (2018) STED super-resolved microscopy. *Nat Methods* 15, 173–182

84 Angibaud, J. *et al.* (2020) A simple tissue clearing method for increasing the depth penetration of STED microscopy of fixed brain slices. *J. Phys. D: Appl. Phys.* 53, 184001

85 Komis, G. *et al.* (2015) Super-resolution Microscopy in Plant Cell Imaging. *Trends in Plant Science* 20, 834–843
86 Rae, A.E. *et al.* (2021) New methods for confocal imaging of infection threads in crop and model legumes. *Plant Methods* 17, 24
87 Johnson, D.C. *et al.* (2005) Structure, Function, and Formation of Biological Iron-Sulfur Clusters. *Annual Review of Biochemistry* 74, 247–281
88 Messal, H.A. *et al.* (2021) Antigen retrieval and clearing for whole-organ immunofluorescence by FLASH. *Nat Protoc* 16, 239–262
89 Avilov, S.V. (2021) Navigating across multi-dimensional space of tissue clearing parameters. *Methods Appl. Fluoresc.* 9, 022001
90 Vieites-Prado, A. and Renier, N. (2021) Tissue clearing and 3D imaging in developmental biology. *Development* 148, dev199369
91 Gusachenko, I. *et al.* (2017) Multimode fibre based imaging for optically cleared samples. *Biomed. Opt. Express* 8, 5179
92 Dent, J.A. *et al.* A whole-mount immunocytochemical analysis of the expression of the intermediate filament protein vimentin in Xenopus.
93 Morley, T. (1968) Accelerated Clearing of Plant Leaves by NaOH in Association with Oxygen. S*tain Technology* 43, 315–319
94 Reynaud, E.G. *et al.* (2015) Guide to light-sheet microscopy for adventurous biologists. *Nat Methods* 12, 30–34
95 Voie, A.H. *et al.* (1993) Orthogonal-plane fluorescence optical sectioning: Three-dimensional imaging of macroscopic biological specimens. *Journal of Microscopy* 170, 229–236
96 Stelzer, E.H.K. and Lindek, S. (1994) Fundamental reduction of the observation volume in far-field light microscopy by detection orthogonal to the illumination axis: confocal theta microscopy. *Optics Communications* 111, 536–547
97 Huisken, J. (2004) Optical Sectioning Deep Inside Live Embryos by Selective Plane Illumination Microscopy. *Science* 305, 1007–1009
98 Ricci, P. *et al.* (2021) Removing striping artifacts in light-sheet fluorescence microscopy: a review. *Progress in Biophysics and Molecular Biology* DOI: 10.1016/j.pbiomolbio.2021.07.003
99 Masters, B.R. (2020) *Superresolution Optical Microscopy: The Quest for Enhanced Resolution and Contrast*, 227Springer International Publishing.
100 Kromm, D. *et al.* (2016) An eye on light-sheet microscopy. In *Methods in Cell Biology* 133pp. 105–123, Elsevier
101 Ovečka, M. *et al.* (2018) Multiscale imaging of plant development by light-sheet fluorescence microscopy. *Nature Plants* 4, 639–650
102 Chakraborty, T. *et al.* (2019) Light-sheet microscopy of cleared tissues with isotropic, subcellular resolution. *Nat Methods* 16, 1109–1113

Glossary

Benzyl Benzoate/Benzyl Alcohol (BABB): mixture is the precursor of all organic solvent-based protocol in animals [5,90].

CLARITY: a protocol designed to render a tissue optically transparent and permeable to macromolecules while keeping its shape using hydrogel embedding [54].

CMF3: a commercial mounting medium with a high RI (1.518) used as clearing agent and suitable with fluorescent immunolabelling [74].

Fluorescent Probe (FP): refers to all fluorescent makers (exo- and endo-genous). Here, in the review, "endogenous FP" specifically refers to encoded fluorescent proteins.

pseudo-Schiff reagents: Schiff reagents are histochemical reagents used to detect aldehydes functions in a tissue after a reaction with a dye containing an amine group. In Pseudo-schiff reactions, imine and aminal groups of chemical dyes react with aldehydes of the tissue, inducing a color change. Five classes of chemical dyes were defined according to the chemical reaction [87]. Non-fluorescent dye except combining with propidium iodide (mPS-PI).

Point Spread Function (PSF): mathematically described the image of point through an optical system and is the result of light diffraction and interference. PSF is represented by a 3D interference pattern. The PSF size is defined by its intensity maxima : $\frac{0,61\lambda}{NA}$ in lateral direction (*x,y* plan); $\frac{2\lambda n}{(NA)^2}$ in axial direction (*x,z* plan) (*NA* : numerical aperture of the objective, λ : light wavelength, *n* : RI of the objective lens). According to Reyleigh criterion, these sizes give the distance that two points have to be separated by to be resolved. As PSF is larger in the axial direction than in the lateral direction (where it respects an Airy diffraction pattern), the lateral resolution of an optical system, is better than its axial resolution.

Refractive Index (RI): is a dimensionless value, often write *n*, indicating the deviation of light encountering a material. *n* is defined as the speed of light in vacuum (*c*) divided by the speed of light in transparent material (*v*), $n = \frac{c}{v}$.

Stimulated Raman Scattering (SRS): belonging, with Coherent anti-Stokes Raman Scattering (CARS) to Coherent Raman Scattering (CRS) microscopy. Here, a sample is simultaneously excited with two laser beams. When the difference of frequency between the two beams corresponds to the frequency of a chemical bond vibrational, there is an amplification of Raman signal (4 times) that can be detected [88]. It leads to label-free imaging of molecules and can also be combined with Raman tags (*e.g.* deuterated molecules) [89].

638 **Table 1. Comparison of optical clearing methods applied to plant tissues.**

Protocol name : Clearing Agent	Plant species	Organ	Refractive index of clearing solution	Protocol duration	Chemical treatments	Enzymatic treatment	Staining	Immuno staining	Microscope	Software	Reference	Reference on animal	Advantages/disavantages
Organic solvents													
Chloral hydrate, chloroform	*A. thaliana*	Leaves Seedlings	1.47-1.48	days	Fix. in ethanol acetic acid; perm. NaOH/SDS	Amylase	mPS-PI	No	CLSM, multiphoton	ImageJ, MedINRIA ImageViewer	[12]	[22]	microscope comparison reported/ reagent toxicity, staining step could eliminate protein and nucleaic acid
PFD, PP11	*A. thaliana*	Leaves	1.31	minutes	No	No	SEYFP	No	CLSM + airyscan, two-photons, second harmonic generation, SRS	Zeiss510	[24]	unknown	fast protocol, suitable with a lot of microscopy type/ never re-used in literature
Visikol : confidential	Various	Leaves, Roots	1.44	minutes/ hours	No	No	GUS staining, periodic Acid, Schiff 's reagent, PI, CyclinB1;1-GUS, FM4-64, GFP, Brefeldin A	No	Fluorescent microscope, CLSM, CLSM+airyscan	SP7, Zeiss Zen, ImageJ	[26–28]	[91]	easy to use/ no referenced for volumetric imaging
BABB : benzyl alcohol/benzyl benzoate (or Murray's clear)	*A. thaliana,* various with or without insect	seedlings, leaves, flowers, fruits	1.56	days/ week (months for insect)	Fix. aceton, deh. methanol	No	GUS staining, autofluorescence	No	M-OPT	Matlab, NRecon, VolViewer, Drishti	[30]	[6,92]	very large samples (cm order)/ no FP imaging reported
	A. thaliana, Medicago truncatula	galls, syncytia, nodules, cysts, egg masses		hours/ days	Fix. 3% glutaraldehyde; deh. ethanol		No (glutaraldehyde autofluorescence)		CLSM	LCS	[31]		efficient for clearing dense tissue/ no FP imaging reported
FluoclearBABB : BABB	Mouse	brain	1.56	hours/ days	Fix. 4% PFA; deh. propanol or tert-butanol; basic pH	No	eGFP	No	LSFM, CLSM	Fiji	unknown	[33]	FP imaging with BABB/not yet applied on plant tissue
Methyl salicylate	*Zea mays*	ovaries, delopping seeds	1.538	days	Fix. FAA (various concentrations); deh. ethanol	No	Feulgen staining (acriflavine)	No	CLSM	unknown	[35]	[6,34]	fast protocol/ unsuitable with endogenous FP
	Crassinucellate	flower buds, mature flowers, immature fruits		one day	Fix. FA; perm. aceton; deh. isopropanol	No	rhodamine-phalloidin, Hoescht	No	CLSM	LASX	[36]		
	Various crop species	Root		days	Fix. 4% PFA, 5% DMSO; deh. ethanol	RNAse	PI, GFP	No	stereomicroscope, CLSM	LASX	[37]		
Simple immersion in aqueous solutions													
SeeDB : fructose, α-thioglycerol	*Acer truncatum, Platanus occidentalis, Robinia pseudoacacia, A. thaliana*	Leaves	1.52	days	Fix. FAA (38% FA); deh. in ethanol	No	PI, Calcofluor white	No	CLSM	Bitplane's, Imaris	[39]	[38]	no clearing effect reported
NaOH			unknown									[93]	tiny effect, no transparency
NaClO			unknown									unknown	efficient for depigmentation/ no information concerning tissue content impact
2,2'-thiodiethanol (TDE)	*A. thaliana*	Various	1.42 - 1.52	hours	Fix. 4% PFA	No	GFP-Tdtomato	No	CLSM, two-photons	Fiji	[45]	[41,43]	refractive index linearly proportional to TDE/ inefficient to remove pigments
TOMEI : TDE	*A. thaliana, Oryza sativa*	Various	1.515	hours	Fix. (TOMEI-I) acetic acid : ethanol (TOMEI-II) 4% PFA	No	DAPI, SYBR green I, GFP	No	CLSM+spinning disk, two-photons	ImageJ, FluoRender, Fluoview, MorphoGraphX, MetaMorph	[44]		

iTOMEI: iohexol, caprylyl sulfobetaine	*A. thaliana, Oryza sativa, Marchantia polymorpha*	Seedlings, leaves, shoot apical meristem, gemma, gemma cup	1.518	one day	Fix. 1% FA	No	various endogenous FP, SR2200, Calcofluor White M2R, Evans blue	No	fluorescence stereomicroscope, CLSM, two-photons,	ImageJ, LASX, Imaris	[46]	[47]	efficient to remove pigments/ could impact lipid and protein content
Protein hyperhydration													
ScaleP, Warner's protocol : urea, Triton X100	Various	Various	unknown	days/ weeks	Fix. 4% PFA ; Glutaraldehyde	cellulase, pectolyase (for immulabelling only)	Alexa fluor 594, Calcofluor white, SYTO 13, Citrine-GFP	Yes : anti-b-1,3-glucan (nodules)	Multiphoton, CLSM	Amira 3D, Huygen's	[49]	[48]	based on a systematic chemical compound screening, suitable with a wide range of plant species and organ/ time to clear
ClearSee : urea, sodium deoxycholate, xylitol	*A. thaliana, Physcomitrella patens*	Seedlings, leaves, pistils, gametophores	1.41	days/ weeks	Fix. 4% PFA	No	Various endogenous fluorescent proteins	No	CLSM, Two photons	NIS-Elements AR 4.10 (Nikon) ZEN 2010	[15]		
ePro-ClearSee : idem ClearSee	Various	Leaves, roots			Fix. 3% PFA; delipidation 0,3% Triton X100	cellulase, pectolyase	DAPI	Yes : various antibodies	CLSM + airyscan	Zen 2 '	[56]		
ClearSeeAlpha : ClearSee + sodium sulphite	Various	Leaves	unknown		Fix. 4% PFA	No	mClover	No	Multiphoton, CLSM	NISElements	[57]		
CTR : ClearSeeAlpha	*Vitis vinifera*	Roots		weeks	Fix. 4% PFA, 5% DMSO	cellulase, pectolyase	PI	No	CLSM	LASX	[59]		
Tissue transformation													
PEA-CLARITY : SDS, Boric acid, NaOH	*A. thaliana, Nicotiana tabacum*	leaves	unknown	weeks/months	Fix. 4% PFA; hydrogel embedding	cellulase, xylanase, arabinofuranosidase, pectatolyase, α -amylase	PI, Calcofluor white	Yes : antiRubisco	CLSM	LAS-AF	[61,62]	[60]	tissue permeabilization and stability/ time to clear

639 Fix. : fixation, deh. : dehydration, perm. : permeabilization, PFD : PerFluoroDecalin, CLSM : confocal laser scanning microscope

Figures

Figure I, Box1. Fundamental principles of optical clearing process

Figure 1. Key values of refractive indices. Refractive indices key values. Plant cell components (left) cover a wide range of refractive indices (RI, dimensionless), rendering plant tissue very scattering and challenging to image in photonic microscopy. In order to homogenize RI into plant tissue, diverse clearing agents have been used (right). (TDE : 2,2'-thiodiethanol; SeeDB : See Deep Brain; BABB : Benzyl Benzoate/Benzyl Alcohol).

Figure 2. Taxonomy of clearing protocols for plant tissues. Clearing protocol taxonomy for plant tissues. Adapted from the last update of clearing protocol taxonomy of animal research literature [5], implemented by the fluorescent staining employed. (PFD: PerFluoroDecalin; PP11: perfluoroperhydrophenanthrene; TDE: 2,2'-thiodiethanol; TOMEI: Transparent plant Organ MEthod for Imaging; iTOMEI: improved TOMEI; ePro-ClearSee: enzymes 2-Propanol ClearSee; CTR: Clearing Tannic Roots; PEA-CLARITY : Plant-Enzyme-Assisted-CLARITY). Description of each protocol in the main text.

Box 1. Clearing process

Plant tissues present a wide diversity of cell types (*e.g*. parenchyma cells, epidermis cells), organelles (*e.g*. chloroplasts, amyloplasts) and components (*e.g*. waxes, pigments). Each of these has its own optical properties and can impede the path of light through the tissue layers. Two major optical phenomena are involved: absorption and scattering.

Light absorption is a loss of photons: their energy is absorbed by molecules. Pigments absorb in the visible spectrum and are more represented in plant kingdom than in any other kingdom. A key process in the clearing of plant tissue consists in reducing absorption by eliminating pigments (Figure I).

Light scattering is the deviation of photons from their straight trajectory when they encounter a medium with a different **Refractive Index** (**RI**). It is a very important parameter in optical fluorescence microscopy, and it is described by the law of refraction. Thus, if a photon is too deviated, it cannot be detected and the signal is lost. In plant tissues, RI range

from 1.00 (air cavities) to 1.61 (lignin [17]). Consequently, the thicker the sample, the higher the scattering events. Hence, in-depth observation is limited to 50 µm in leaf tissue [15]. The major process of the CP is the homogenization of RI throughout the entire tissue (Figure I).

Because the optical properties of a tissue are dependent on its specific composition, CPs have to be optimized not only according to species (*e.g*. moss ≠ tree), but also according to tissues (*e.g*. leaf ≠ root), and to microscopy techniques (see section 2 and Box 2).

Box 2. A focus on light sheet fluorescence microscopy

The development of **Light Sheet Fluorescence Microscopy** (**LSFM**) was a breakthrough innovation in optical sectioning [94]. In LSFM, the specimen is illuminated by a sheet of light perpendicular to the detection system, and the centre of the light sheet matches the focal plane. The main advantage is that fluorophores outside this plane are not illuminated, so that noise and phototoxicity are lower. But, the system is highly sensitive to scattering and absorption because photons emitted in the focal plane must travel through the rest of the tissue before reaching the objective. Moreover, a specific mounting system is required regarding the angle of illumination, and mostly involves fixing a piece or an entire specimen onto a support.

This planar illumination combined with a fluorescent signal were first developed under the name Orthogonal-Plane Fluorescence Optical Sectioning (OPFOS [95]). Faced with the opacity of bones, the first guinea pig cochlea observed under a light sheet microscope was cleared using Spalteholz clearing agent. This first LSFM was developed with a CP, promising joined developments between microscopy techniques and sample preparation. A device combining perpendicular illumination plant and point scanning confocal microscopy was developed and gave a better axial resolution than ordinary confocal microscopy [96]. In 2004, Huisken and colleagues [97] optimized their instrument by using wide-field detection instead of confocal detection: Selective Plane Illumination Microscopy (SPIM) was born, and modern LSFM in its wake. Meanwhile, the popularity of LSFM increase and developments of the technique stemmed from homebuilders scientists and instrumentals companies to the point that in 2014, LSFM was recognized as “method of the year” by the journal *Nature*.

LSFM implementations concerned illumination and detection optics (*e.g.* two sides illuminations, two detection paths, upright or inverted, four paths used at detection and illumination, multidirectional illumination). Moreover, standard Gaussian beam light sheet has been modified to enhanced LFSM performances (*e.g.* digitally-scanned laser light-sheet, light coherence controlled; coupled with two-photons or multiphoton illumination; replaced by self-reconstructing beams, lattice light sheet, infrared light sheet) [98]. These enhancements lead to the homogenization of illumination; corrections of the shadow effect and stripes artefacts; increasing imaging speed, resolution and depth penetration. In 2020, Masters [99] published an insightful book about super-resolution microscopy in which advances in LSFM were well described and discussed. Moreover, numerical post-processing treatments exist to improve image quality [98]. Among all LSFM set-up available nowadays, it is really important to choose one that suits the biological cleared sample and the experimental interest [100].

Concerning plant research, a review by Ovečka and colleagues [101] presents and discusses plant development imaging by LSFM. Most of publications on plant tissue imaged by LSFM concern *in vivo* acquisition. Even though some publications are now dedicated to LSFM on cleared samples [102], none has yet addressed cleared plant tissues.

Figure 1

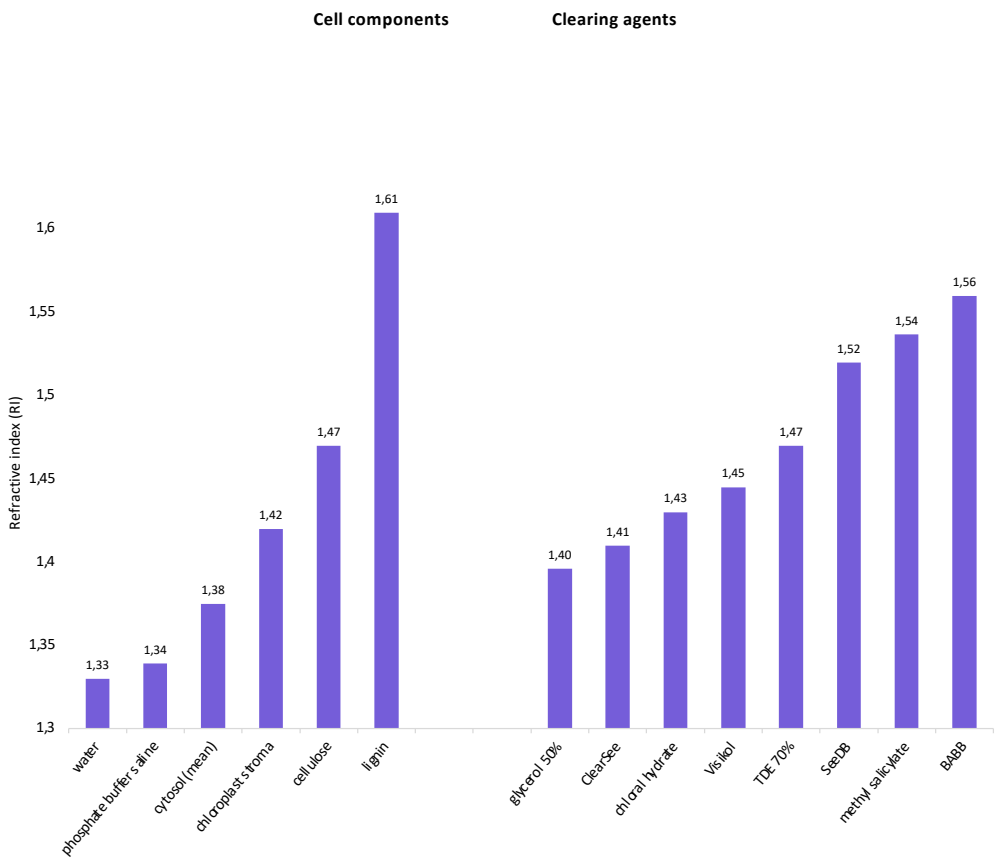
Cell components
Clearing agents
Refractive index (RI)
1,6
1,55
1,5
1,45
1,4
1,35
1,3
1,33
1,34
1,38
1,42
1,47
1,61
1,40
1,41
1,43
1,45
1,47
1,52
1,54
1,56
water
phosphate buffer saline
cytosol (mean)
chloroplast stroma
cellulose
lignin
glycerol 50%
ClearSee
chloral hydrate
Visikol
TDE 70%
SeeDB
methyl salicylate
BABB

Clearing protocols for plant tissues

- Organic solvents
  - PFD, PP11
  - Methyl salicylate
  - Visikol
- Immersion in aqueous solutions
  - NaClO
  - TDE
    - TOMEI
      - iTOMEI
- Hyperhydrating solutions
  - Warner's protocol
    - ClearSee
      - ePro-ClearSee
      - ClearSeeAlpha
      - CTR
- Tissue transformation
  - PEA-CLARITY